

BL Lac Objects in the Synchrotron Proton Blazar Model

A. Mücke^{a,1}, R.J. Protheroe^b, R. Engel^c, J.P. Rachen^{d,2} & T. Stanev^c

^aDépartement de Physique

Université de Montreal, Montreal, QC, H3C 3J7, Canada

^bDepartment of Physics and Mathematical Physics

The University of Adelaide, Adelaide, SA 5005, Australia

^cBartol Research Institute, University of Delaware, Newark, DE 19716, USA

^dSterrenkundig Instituut, Universiteit Utrecht, 3508 TA Utrecht, The Netherlands

Abstract

We calculate the spectral energy distribution (SED) of electromagnetic radiation and the spectrum of high energy neutrinos from BL Lac objects in the context of the Synchrotron Proton Blazar Model. In this model, the high energy hump of the SED is due to accelerated protons, while most of the low energy hump is due to synchrotron radiation by co-accelerated electrons. To accelerate protons to sufficiently high energies to produce the high energy hump, rather high magnetic fields are required. Assuming reasonable emission region volumes and Doppler factors, we then find that in low-frequency peaked BL Lacs (LBLs), which have higher luminosities than high-frequency peaked BL Lacs (HBLs), there is a significant contribution to the high frequency hump of the SED from pion photoproduction and subsequent cascading, including synchrotron radiation by muons. In contrast, in HBLs we find that the high frequency hump of the SED is dominated by proton synchrotron radiation. We are able to model the SED of typical LBLs and HBLs, and to model the famous 1997 flare of Markarian 501. We also calculate the expected neutrino output of typical BL Lac objects, and estimate the diffuse neutrino intensity due to all BL Lacs. Because pion photoproduction is inefficient in HBLs, as protons lose energy predominantly by synchrotron radiation, the contribution of LBLs dominates the diffuse neutrino intensity. We suggest that nearby LBLs may well be observable with future high-sensitivity TeV gamma-ray telescopes.

PACS: 98.70 Rz, 98.54 Cm, 95.30 Gv, 98.58 Fd, 98.70 Sa, 98.70 Vc

Keywords: Active Galaxies: Blazars, BL Lac Objects: general,
Gamma-rays: theory, Neutrinos, Synchrotron emission, Cascade simulation

¹present address: Ruhr-Universität Bochum, Institut für Theoretische Physik, Lehrstuhl IV: Weltraum- und Astrophysik, D-44780 Bochum, Germany
email: *afm@tp4.ruhr-uni-bochum.de*

²present address: T-Systems GEI GmbH, Munich, Germany
email: *Joerg.Rachen@t-systems.com*

1 Introduction

Blazars are identified as Optically Violent Variable (OVV) quasars (a sub-class of Flat Spectrum Radio Quasars, FSRQ) and BL Lacs which may be low-frequency or high-frequency peaked BL Lac objects. Their broad-band spectra consist of two spectral components which appear as broad ‘humps’ in the spectral energy distribution, and are due to emission from a jet oriented at small angle with respect to the line-of-sight. The low-energy component is generally believed to be synchrotron emission from relativistic electrons, and extends from the radio to UV or X-ray frequencies. The origin of the high-energy component, from X-ray to γ -ray energies, in some cases to several TeV, is still under debate.

Various models have been proposed, with the most popular ones being the “leptonic models”, where a relativistic electron-positron jet plasma up-scatters low energy photons to high energies via the Inverse Compton effect. The emission region moves with relativistic velocities along the jet, and the resulting radiation is highly beamed into the observer’s line-of-sight. The target photon field could come either from the accretion disk surrounding the putative black hole (e.g. [1, 2]), possibly partly reprocessed by broad-line region (BLR) clouds (e.g. [3]) or a dusty torus (e.g. [4], [5]), or it could be produced by the relativistic e^\pm population itself, in so-called synchrotron - self Compton (SSC) models [6, 7]. In such leptonic models, it seems plausible to assume that SSC radiation dominates in objects with relatively weak accretion disk radiation such as BL Lac objects, while in FSRQs external photons provide the dominant target field for the Inverse Compton process.

As an alternative to leptonic models, “hadronic models” were proposed more than 10 years ago to explain the γ -ray emission from blazars [8, 9]. Recently Mücke & Protheroe [10, 11] have discussed in detail the various contributing emission processes. In hadronic models the relativistic jet consists of relativistic proton and electron components, which again move relativistically along the jet. High-energy radiation is produced through photomeson production, and through proton and muon synchrotron radiation, and subsequent synchrotron-pair cascading in the highly magnetized environment. Again either external (i.e. from an accretion disk and/or IR-torus [13]) or internal photon fields (i.e. produced by synchrotron radiation from the co-accelerated electrons) can serve as the target for photopion production. Gamma-ray loud BL Lac objects are most likely explained by the latter possibility. These models can, in principle, be distinguished from the leptonic models by the observation of high energy neutrinos generated in decay chains of mesons created in the photoproduction interactions (for a recent review see [14]).

In this paper, we study the properties of the Synchrotron Proton Blazar (SPB) model [11], where the dominant target photon field is produced by directly accelerated electrons that manifests itself in the blazar SED as the synchrotron hump. A detailed description of the model itself and its implementation as a Monte-Carlo/numerical code has already been given in [11]. Since this model is for objects with a negligible external component of the radiation field in the jet, we apply it only to BL Lac objects. It has been successfully

demonstrated that this model reproduces well the observed double-humped blazar SED. The goal of this paper is to present a comprehensive study of the model’s parameter space, a promising tool for discriminating between leptonic models and the hadronic SPB-model. We apply our model to both LBLs and HBLs, and discuss our results in the light of the suggested LBL/HBL continuity.

In Section 2 we give a brief description of the SPB model. The model is applied to HBLs and LBLs to calculate the SEDs in Section 3. We vary the magnetic field strength and the target photon density and study their effect on the resulting cascade spectrum. These results are used to identify the parameter sets within the SPB-model which are typical for HBLs and LBLs in Sect. 3.2. In Sect. 3.3 we compare the model predictions to observed SEDs from HBLs and LBLs. One of the most dramatic properties of blazars is their variability, and this issue is addressed by modeling the evolution of the SEDs during outburst and quiescent stages in Sect. 3.4. The predicted neutrino emission from these sources is calculated in Section 4. Finally, we discuss our results in Sect. 5.

2 The model

We consider an emission region, or “blob”, in an AGN jet which moves relativistically along the jet axis which is closely aligned with our line-of-sight. The model assumes that electrons (e^-) and protons (p) are co-accelerated at the same site in the jet. Due to pitch-angle scattering the resulting particle distributions are expected to be quasi-isotropic. The energetic protons, which follow a power law energy spectrum, are injected instantaneously into a highly magnetized environment, and suffer from energy losses due to proton–photon interactions (meson production and Bethe-Heitler pair production), synchrotron radiation and adiabatic expansion. The mesons produced in photomeson interactions always decay in astrophysical environments. For the magnetic fields and proton energies typically assumed in hadronic blazar models, however, secondary particles such as mesons and muons may suffer synchrotron losses before they decay [12], and this is also taken into account. The relativistic co-accelerated e^- radiate synchrotron photons that serve as the target radiation field for proton-photon interactions and the pair-synchrotron cascade which subsequently develops. This cascade redistributes the photon power to lower energies where the photons eventually escape from the emission region. The cascades can be initiated by photons from π^0 -decay (“ π^0 cascade”), electrons from the $\pi^\pm \rightarrow \mu^\pm \rightarrow e^\pm$ decay (“ π^\pm cascade”), p -synchrotron photons (“ p -synchrotron cascade”), charged μ^- , π^- [12] and K -synchrotron photons (“ μ^\pm -synchrotron cascade”) and e^\pm from the proton-photon Bethe-Heitler pair production (“Bethe-Heitler cascade”). The probability of pair production is calculated from the $\gamma\gamma$ pair production opacity. The e^+e^- -pairs generated radiate synchrotron photons, which again suffer from pair production, and feed the cascade development. We use the matrix method (e.g. [15]) for simulating the developing cascades. Our model utilizes exact cross sections pre-calculated using the Monte-Carlo technique. This is especially important for the hadronic particle production. The photomeson production is simulated with the SOPHIA Monte-Carlo code [16]. Details of the model implementation,

e.g. energy loss rates, cascading method, etc., are described in [11].

The “ π^0 cascades” and “ π^\pm cascades” generate rather featureless photon spectra in contrast to “ p -synchrotron cascades” and “ μ^\pm -synchrotron cascades” that produce a double-humped SED as typically observed for γ -ray blazars. We find the contribution from Bethe-Heitler pair production to be negligible. Direct proton and muon synchrotron radiation is mainly responsible for the high energy hump whereas the low energy hump is dominated by synchrotron radiation by the directly accelerated e^- , with a contribution of synchrotron radiation from secondary electrons (produced by the p - and μ^\pm -synchrotron cascade).

In the present paper, we have made three changes to the original model. The first change addresses e^+e^- pair production in photon-photon collisions. Due to energy and momentum conservation, one of the produced pair electrons (with energy E_{e+} , E_{e-}) carries most of the available energy. We take this into account by using $E_{e+} = 0.1E_\gamma$, whereas the original model assumed that $E_{e+} = E_{e-} = 0.5E_\gamma$. Test runs show that the effect of this improvement on the cascade development is very modest.

The second change in the model concerns the particle acceleration time scale. In the most general form it can be written as

$$t'_{\text{acc}} = \frac{\gamma' mc^2}{\eta ec^2 B'} \quad (1)$$

for almost all proposed particle acceleration scenarios, with $\eta \leq 1$ being the acceleration efficiency which is strongly model dependent and, in most cases, even not well defined. Hence, instead of specifying η , and thereby limiting ourselves to one specific scenario, we use Eq. (1), and leave η as a free parameter. The efficiency, η , essentially influences the cutoff energy of the accelerated particle spectrum which is obtained by balancing the loss and gain time scales. The particle spectrum is assumed to follow a Heaviside function at the cutoff energy.

The third change concerns the treatment of the size of the emission region R' . In this paper we use R' as a free parameter, independent of the variability time scale. The justification for this is given in [17] which discuss the relation between the emission region geometry and the observed variability time. Note that in blazar models where protons are picked up from the ambient medium by a relativistic blast wave, the so-called “pick-up models” [18], the variability time scale is determined by density inhomogeneities in the ambient medium rather by the size of the emission region. The value of R' is relevant for the $\gamma\gamma$ pair production opacity, $p\gamma$ interaction rate, $n\gamma$ opacity, adiabatic losses due to jet expansion (see Appendix A) and the normalization of the emitted cascade spectrum.

Because of the high energy threshold for photoproduction, hadronic models require extremely high proton energies which can only be achieved in a highly magnetized environment, and so synchrotron losses become very severe. Magnetic field values of order 10^4 G are expected near the horizon of a supermassive black hole with mass $10^8 - 10^9 M_\odot$ [19]. Assuming magnetic flux conservation, jet magnetic fields may reach values of 1-100 G in an emission region $\simeq 100 - 1000$ AU away from the black hole horizon.

Throughout this paper we assume that the injected and accelerated particle spectrum can be represented as a power-law spectrum $n'_p \propto \gamma'^{-\alpha_p}$, $\gamma'_{p1} \leq \gamma'_p \leq \gamma'_{p2}$ and we use $\alpha_p = 2$ and $\eta = 1$ unless noted otherwise. In the following all quantities in the jet frame are indicated by a prime, while quantities in the observer's frame are unprimed.

3 Applications

3.1 Observations of HBL and LBL

Gamma-ray loud BL Lac objects are commonly classified as HBLs or LBLs on the basis of their ratio of radio to X-ray flux i.e. HBLs have a broad-band spectral index $\alpha_{\text{RX}} \leq 0.75$ and LBLs have $\alpha_{\text{RX}} > 0.75$ [20]. Consequently, for the LBL sub-class, the synchrotron peak is generally observed at IR/optical/UV-frequencies, while the X-ray band covers the local minimum of the SED νL_ν between the two spectral humps. LBLs were thought to represent an intermediate object class between FSRQs, which have much higher bolometric luminosities, and HBLs, which are the least luminous blazars. In FSRQs νL_ν peaks in the IR/optical/UV and at MeV-GeV-energies, while in HBLs νL_ν peaks at soft to medium-energy X-rays and GeV-TeV energies. The apparent strict bimodality in the BL Lac distribution seems, however, now to be replaced by a more continuous scenario. New surveys such as DXRBS [21], RGB [22] and REX [23], which cover previously unexplored regions in the parameter space, show a smoother distribution of peak frequencies, suggesting that the two classes of objects are not intrinsically different, but result from one or a few parameters varying within the *same* source population.

In order to identify the critical parameter(s) in the framework of the SPB-model we have constructed the “average” synchrotron spectrum for each class, HBLs and LBLs, which serve as the target photon distribution for our cascade model. For this undertaking we use the “average” of an extensive collection of blazar SEDs published by Ghisellini et al. [24]. By overlaying all available HBL and LBL SEDs we find that the following broken power law gives a reasonable representation of the low-frequency hump in the SED of HBLs and LBLs

$$n(\epsilon) \propto \begin{cases} \epsilon^{-\alpha_1} & \text{for } \epsilon_i \leq \epsilon \leq \epsilon_b \\ \epsilon^{-\alpha_2} & \text{for } \epsilon_b \leq \epsilon \leq \epsilon_c \end{cases} \quad (2)$$

with $\alpha_1 = 1.5$, $\alpha_2 = 2.25$ and $\epsilon_i = 10^{-5} \dots 10^{-6}$ eV. The break may be considered as a result of emission by an electron spectrum that is dominated by expansion losses below the break energy, and by synchrotron losses above (see e.g. [9]). The parametrizations for each object class are visualized in Fig. 1. We find that the break energy ϵ_b of LBLs varies up to about one order of magnitude, from ≈ 0.1 eV to 1.3 eV, while the maximum synchrotron photon energy ϵ_c can cover a range up to two orders of magnitude, from ~ 41 eV to 4 keV. The populated energy range of HBLs is more restricted: $\epsilon_b \approx 26$ eV to 131 eV and $\epsilon_c \approx 4.1$ keV to 41 keV. The peak of the low-energy SED is $\log \nu L_\nu^{\text{max}}(\text{erg/s}) \approx 45.6 - 46.1$ for LBLs and $\log \nu L_\nu^{\text{max}}(\text{erg/s}) \approx 43.4 - 43.8$ for HBLs. We define the “standard LBL” by $\epsilon_b = 1.3$ eV, $\epsilon_c = 4.1$ keV and $\log \nu L_\nu^{\text{max}}(\text{erg/s}) = 46.1$, and the “standard HBL” by $\epsilon_b = 131$

eV, $\epsilon_c = 41$ keV and $\log \nu L_\nu^{\max}(\text{erg/s}) = 43.8$. In the following parameter study, we use these “definitions”, and vary the magnetic field strength and target photon density as the most interesting parameters.

3.2 Parameter study

In this section we explore the effects of varying different model parameters on the blazar SED, especially its high-energy part.

3.2.1 Magnetic field strength

The magnetic field is a key parameter in hadronic models. In order to accelerate protons to energies above the photopion production threshold, fields of order 10 G are necessary. Fig. 2 shows the resulting SED for “standard” HBL and LBL target photon spectra in a 10, 30 and 50 G field. If HBLs possess intrinsically low photon fields, proton synchrotron radiation always dominates over pion production. The resulting cascade spectrum (Fig. 2a) consists mainly of proton synchrotron emission at gamma-ray energies, and reprocessed proton synchrotron radiation (i.e. synchrotron radiation from the pair produced e^\pm) at X-ray energies for $B' \geq 10$ G.

In the denser (LBL-like; see Sect. 3.2.2) photon fields one can observe the growing importance of synchrotron losses with increasing magnetic field strength. Synchrotron radiation generates two distinct humps: one at high energy mainly due to the emerging μ synchrotron radiation, and one at low energy dominated by synchrotron radiation of the secondary electrons from the μ synchrotron cascade. The radiation from the π^0 and π^\pm -cascades adds to the emission from the p and μ synchrotron cascades, and so may fill in the gap between the two humps, especially for low magnetic fields. For field values below 10 G, the featureless π^0 and π^\pm -cascades may even dominate the emerging cascade spectrum. This highlights the need of high field values in blazars in the framework of the present model.

Muon synchrotron radiation, and its subsequent generation(s), peaks at higher energies than the corresponding p synchrotron radiation [25]. Aharonian [26] has argued that a significant flux of TeV-photons requires an optically thin emission region at these energies, thus a low target photon density and consequently a low efficiency of photopion production. In TeV blazars, all of which are HBLs, we therefore expect the contribution from the μ synchrotron cascade to be smaller than that from the p synchrotron cascade. (Note, however, that the spectral data may be also explainable by models with a moderately optically thick photospheric emission in the TeV-regime [9] which would allow a higher photohadronic interaction rate and observable emission of π^0 and μ -induced cascades also in TeV-blazars [25].) However, it seems to be the opposite in LBLs. Here, for field values up to at least 50 G the μ synchrotron cascade determines the 2-peak structure in our chosen “standard” LBL, while a non-negligible contribution from the π -cascades fills the gap between the humps in the SED, smoothing out the bumpy spectral shape.

We find that with increasing magnetic field, the two-humped structure becomes more and more pronounced due to the growing μ and p synchrotron photon production, and the luminosity increases partly because we have assumed that the relativistic proton energy density increases in equipartition with magnetic field energy density.

The ratio between the low to high energy peak of the cascade spectrum is mainly determined by opacity effects, and is in general lower in the denser LBL-like target photon fields than in the less dense HBL-like environments, as seen in Fig. 2.

The maximum photon energy in the high-energy hump is proportional to $\gamma'_{p,\max}{}^2 B' D$ where $\gamma'_{p,\max}$ is the maximum proton Lorentz factor, which in turn is determined by balancing the acceleration time scale with the energy loss scale, and D is the Doppler factor. In HBLs this particle cutoff is caused by p synchrotron losses for strong fields, and adiabatic losses for fields $B' \leq 10$ G. In the denser target photon fields of LBLs the cutoff occurs at significantly lower energies, and is caused by losses through photopion production, independently of magnetic field strength.

3.2.2 Jet-frame target photon field

So far, there is no convincing evidence for significantly different Doppler factors and emission volumes in HBLs and LBLs. As a consequence, the more luminous LBLs probably possess larger co-moving frame electron synchrotron photon densities than HBLs. In this section we study the effect of varying the target photon density on the high-energy hump of the SED in the SPB-model.

Fig. 3a shows the cascade spectrum in a HBL-like target photon distribution with varying low-energy target photon density indicated in the figure as the broken power law curves at the left. The size of the emission region R' , Doppler factor D and magnetic field B' are held fixed at $D = 10$, $R' = 5 \times 10^{15}$ cm and $B' = 30$ G. For these fixed parameters, $u'_{\text{phot}} = 10^8$ – 10^{11} eV cm $^{-3}$ covers the full range of observed νL_ν in HBLs as described in Sect. 3.1, and we shall describe the effect of varying u'_{phot} in this range. As mentioned previously, the contribution of μ -synchrotron and π -cascades increases with increasing u'_{phot} because of the growing efficiency of photo-meson production. This affects not only the shape of the cascade spectrum, but also the proton cutoff energy. Specifically, in Fig. 3a the proton spectrum cuts off due proton synchrotron losses for $u'_{\text{phot}} \leq 10^{11}$ eV cm $^{-3}$. The corresponding cascade spectra are mainly determined by the p synchrotron cascade. For higher u'_{phot} a significant contribution from the μ -cascade emission modifies the spectral shape. The apparent increase of the “dip” energy (i.e., the energy corresponding to the minimum between the low and high energy humps of the *cascade* spectrum) with increasing u'_{phot} above 10^{10} eV cm $^{-3}$ is caused by an increase in the reprocessed μ synchrotron component. Because opacity effects also gain importance for higher photon densities, the ratio of the low to high energy peaks of the cascade SED increases with increasing u'_{phot} . It is interesting to note that the soft photon and high energy peak luminosities are approximately equal for target densities $u'_{\text{phot}} \approx 10^{10} \dots 10^{11}$ eV cm $^{-3}$, and their ratio increases with increasing target photon density.

Keeping R' , D and B' fixed as before, and increasing the target photon density even more, one enters the range for LBL-like blazars: $u'_{\text{phot}} = 10^{11}\text{--}10^{14}$ eV cm³ would correspond to $\nu L_{\text{max,syn}} = 10^{45}\text{--}10^{48}$ erg/s. The predicted LBL cascade spectra are shown in Fig. 3b. Clearly visible is the decrease of the high-energy cutoff with growing u'_{phot} . Here, energy gains from acceleration are balanced by photoproduction losses in all cases. Because of the dense target photon fields, photo-meson production determines not only the cutoff energy but also the spectral shape. Opacity effects are responsible for the steady decline of the high energy hump with increasing u'_{phot} as more and more energy is redistributed from high to low energies. The dip energy, and corresponding dip luminosity, then become increasingly difficult to define. The reprocessed μ synchrotron radiation, which initially dominates the low energy hump of the cascade spectrum, is gradually replaced by the featureless π -cascade emission for $u'_{\text{phot}} \geq 10^{11}$ eV cm⁻³ which fills the gap between the low and high-energy cascade humps. The π cascade dominates the emission between 1 MeV and 100 MeV for $u'_{\text{phot}} = 10^{12}$ eV cm⁻³, and between 10 keV and 100 MeV for $u'_{\text{phot}} = 10^{13}$ eV cm⁻³ in LBL-like target spectra. For denser target photon fields the π cascades completely determine the whole cascade spectrum, and proton synchrotron radiation would be unimportant.

To summarize, in the low target photon densities of HBL-like objects p synchrotron radiation and its reprocessed emission dominates. In the very dense target photon environments of LBL-like sources photo-meson production becomes so efficient that first μ synchrotron cascade radiation, and finally π -cascade radiation determines the entire cascade SED.

The radiative efficiency of photopion production is much lower than p synchrotron radiation, and this becomes apparent when comparing Fig. 3a and 3b. SEDs dominated by p synchrotron radiation show in their high-frequency humps power comparable to or higher than the seed photon density (mainly generated by synchrotron emission from primary electrons). However, when photoproduction is the dominant process, the emerging cascade spectra are significantly below the low energy hump caused by the directly accelerated electrons. Thus, if LBL-like objects have high density target photon fields $u'_{\text{phot}} \geq 10^{11}$ eV cm⁻³, then they would be γ -ray quiet unless one of the other parameters (e.g. D , R' , B') changed in a way to increase the high-frequency hump. Indeed, this could explain why many radio-loud blazars have never been observed in γ -rays. Intrinsic TeV-emission from LBLs could also be suppressed if the particle acceleration efficiency η is significantly lower than for HBLs.

The effects of varying the size of the emission region R' and/or D for a given magnetic field and target photon density are obvious: an increase in R' and/or D would result in a significant increase in the emerging luminosity, and the maximum photon energy would increase with increasing Doppler factor. Furthermore, since the photon-photon pair production opacity $\tau_{\gamma\gamma} \propto u'_{\text{phot}} R'$ grows with the size of the emission region, it will cause effects similar to increasing u'_{phot} without, however, any change of the $p\gamma$ interaction rate.

An interesting case is when proton synchrotron and photoproduction losses are approx-

imately equal above the pion production threshold. This occurs, e.g., at target photon densities $u'_{\text{phot}} \approx 10^{11} \text{ eV cm}^{-3}$ for a 30 G magnetic field (see Fig. 4a). Because the break energy in the low energy synchrotron component (used as target for $p\gamma$ interactions in our model) is low in LBLs, the pion production loss time follows roughly a $\gamma'_p{}^{-1.25}$ dependence up to $\gamma'_p \sim 10^9$, and is at roughly the same level as the proton synchrotron loss time $\gamma'_p{}^{-1}$ from low to high proton energies. This leads for the given parameters to approximately equal pion production and proton synchrotron losses at high energies in LBL. The rather dense target photon field, together with a strong magnetic field, are ideal conditions for muon synchrotron radiation. Consequently, in LBLs with $B' \approx 30 \text{ G}$ and $u'_{\text{phot}} \approx 10^{11} \text{ eV cm}^{-3}$, the high energy hump is mainly due to proton and muon synchrotron radiation (see Fig. 4a). In contrast, HBLs have much higher break energies in their low energy synchrotron component, with the consequence that proton synchrotron losses dominate over pion production losses, leading to a high-frequency hump which is predominantly due to proton synchrotron radiation (see Fig. 4b).

3.3 The LBL/HBL continuity in the SPB model – a comparison with the observations

In this section we propose that HBLs and LBLs are intrinsically the same objects but with different low energy photon densities u'_{phot} . The photon density may range continuously from low (HBLs) to high (LBLs) values, resulting in a continuous range of SEDs in the low energy hump, consistent with the apparent strict bimodality in the BL Lac distribution being now replaced by a more continuous scenario as suggested following recent data from DXRBS [21], RGB [22] and REX [23]. Because for each parameter set in the SPB model there exists a u'_{phot} above which $p\gamma$ interactions dominate, and below which proton synchrotron losses dominate, this results in a dichotomy when the high energy hump is included in the SED. Thus, while there is apparently continuity at low energies, we suggest there is nevertheless a dichotomy at gamma-ray energies.

We first discuss an example corresponding to an extreme HBL. Fig. 5a shows the relevant time scales for a relatively low target photon density of $u'_{\text{phot}} \approx 10^9 \text{ eV cm}^{-3}$, and Fig. 5b shows the various cascade components. The clear dominance of the p synchrotron radiation at high energies is obvious, the low energy component is reprocessed proton synchrotron emission with a peak luminosity which is significantly lower than that of the high-energy hump. For much lower target photon fields, $u'_{\text{phot}} \leq 10^8 \text{ eV cm}^{-3}$, the probability for p synchrotron photons to produce e^\pm pairs is negligible, and thus reprocessed proton synchrotron radiation does not appear. Bethe-Heitler pair production and pion photoproduction are also unimportant, as is the μ synchrotron cascade. Because of the low target photon density in the emitting volume, photons up to several TeV can escape the emission region.

Fig. 6 shows an example corresponding to an extreme LBL, i.e., at the other end of the BL Lac distribution. Losses due to photo-meson production cut the proton injection spectrum off at $\gamma'_{p,\text{max}} \approx 10^9$ (see Fig. 6a), with the consequence that only photons up

to several tens of GeV are important in the cascade spectrum (Fig. 6b). With p synchrotron radiation being rather unimportant in this environment, the cascades initiated by photo-pion production completely dominate the SED, and produce a rather featureless spectrum, where the dip between the low- and high energy cascade component has completely disappeared.

To demonstrate the LBL/HBL dichotomy we shall discuss the observed SEDs of a typical HBL (Mkn 421) and a typical LBL (PKS 0716+714) within the framework of our SPB model. The data were taken again from Ref. [24], and thus represent the average SED for both objects. Fig. 7a shows our model fits to the data (corrected for attenuation during propagation through the infrared background [27]). Comparing the observed SED with models shown in Fig. 3, it is immediately apparent that Mkn 421 represents an extreme HBL in the framework of our SPB model. Using a relatively low jet-frame target photon density of $u'_{\text{phot}} \approx 10^9 \text{ eV cm}^{-3}$, the high-energy part of the spectrum is completely determined by p synchrotron radiation. The low-energy hump is dominated by the synchrotron radiation of the directly accelerated electrons. The shape of the target spectrum, a broken power law with spectral indices $\alpha_1 = 1.5$ and $\alpha_2 = 2.25$, is the same as used in Sect. 3.2, but the break energy and normalization has been adjusted to the data. In order to explain the emitted energies of several TeV, the acceleration efficiency must be $\eta \approx 1$. High values of η ($\eta \approx 1$) can realistically be obtained by diffusive shock acceleration [28] or, even more promisingly, by annihilation of magnetic fields [29]. A typical Doppler factor of $D \approx 10$ and emission region radius of $R' = 3 \times 10^{15} \text{ cm}$ has been used for this fit.

PKS 0716+714, classified as an LBL by [24], has been chosen because of its well-defined low-energy synchrotron component. Again, the same power law spectral indices are used as in Sect. 3.2 to represent this component, and the break energy and normalization are adjusted to the data (see Fig. 7b). This blazar has been observed to emit only up to EGRET-energies. Thus a maximum proton Lorentz factor of $\gamma'_{\text{p,max}} \approx 10^9$, determined by pion production losses in our model fit, is enough to explain these energies which can be reached even with modest acceleration efficiencies of $\eta \sim 10^{-2}$.

Within the framework of the SPB-model, PKS 0716+714 has a target photon density of $u'_{\text{phot}} \sim 10^{11} \text{ eV cm}^{-3}$, and seems to lie between LBLs and HBLs. The emission at MeV-energies is dominated by p synchrotron radiation, while the low-energy part of the *cascade* spectrum is mainly due to reprocessed μ synchrotron radiation. The synchrotron radiation from directly accelerated electrons is, however, responsible for the observed low-energy hump. High energy photons up to multi-TeV are expected from PKS 0716+714 due to μ -synchrotron radiation. This would be detectable by high-sensitivity Cherenkov-telescopes such as MAGIC and VERITAS if photon-absorption in the cosmic background radiation field would be negligible for this source, but the unknown redshift (we have assumed here $z = 0.3$ [24]) makes this prediction rather uncertain. However, the MeV-GeV emission predicted from PKS 0716+714 should be definitively detectable by GLAST [30].

3.4 From quiet to flare state in the SPB model

Variability in the present model could be caused by an increase in the accretion rate causing a shock to propagate along the jet. Pre-existing density enhancements or “blobs” could thereby be re-energized, and may undergo an increase in their bulk Lorentz factor.

To demonstrate how this could work in HBLs, we have chosen the γ -ray loud BL Lac object Mkn 501 where the different stages of activity seem to be sampled best [31]. Fig. 8 shows our modeling of the three main activity states (historical, 7 April 1997 and 16 April 1997) leading to the giant 1997-flare. Mkn 501 is an HBL, and so the dominant γ -ray production mechanism in our SPB model should be proton synchrotron emission. This would be the case even for the quiet state, although we note that the high-energy component in this state is not very well constrained, and other parameter choices can easily be found to fit the data equally well. Future data from more sensitive instruments, e.g. GLAST [30], may provide better constraints. For each of the three states, we show the target photon spectrum (solid curves) we use for pion photoproduction, and cascading.

As the shock moves through the highly magnetized plasma, electrons start to increase their synchrotron photon production, possibly due to an increase in the number of relativistic electrons. This leads to a higher *intrinsic* (i.e. jet-frame) photon density, and thus to an increase of the observed synchrotron hump, from $\nu L_{\nu, \text{max}} = 10^{44.2}$ to $10^{44.7}$ to $10^{45.4}$ erg/s for the Mkn 501 1997-outburst. Simultaneously, the number of relativistic protons also increases. The appearance of a “fresh” relativistic shock in an otherwise weakly turbulent plasma implies qualitatively an increase of the acceleration efficiency η . In our model we increased η from $\eta = 0.05$ to $\eta = 1$ during flaring, and this naturally leads to a higher and correlated cutoff energy of both electron and proton particle spectra, and consequently to a *correlated* shift of synchrotron peak energy and γ -ray peak energy to higher energies. We also note that the observed break in the electron synchrotron spectrum becomes less pronounced with flaring activity, as is expected when the energy loss time scale becomes comparable to the dynamical (i.e. light-crossing) time scale for a particle injection spectrum steeper than $\alpha_p \geq 1$ [26]. For simplicity, however, we have used a broken power law spectrum with the same break (i.e. $\alpha_1 = 1.5$, $\alpha_2 = 2$) for all three activity stages to represent the target photon spectrum for our SPB-model. The target photon spectrum break and cutoff energies used were $\epsilon_b = 2$ eV and $\epsilon_c = 4$ keV for the quiescent state, $\epsilon_b = 1$ keV and $\epsilon_c = 160$ keV for the intermediate state, and $\epsilon_b = 40$ keV and $\epsilon_c = 200$ keV for the flaring state.

Due to the higher acceleration efficiency, the cutoff energy in the injected proton spectrum, determined by synchrotron losses, increases by about a factor of 5 in our example. Although the jet frame target photon density increases nearly a factor of five from the quiescent stage to the flare stage, photo-meson production, and thus μ synchrotron emission as proposed in [25] to explain the Mkn 501 flare, remains still of minor importance.

The combined effect of increasing proton cutoff energy, and increasing Doppler factor, causes an increase of the “dip” energy in the blazar SED. This behaviour is also expected for leptonic SSC models (see [31]), as a result of the increasing synchrotron and Compton peak energy and the flattening of the underlying electron spectrum.

The magnetic field and the jet frame emission volume remain approximately constant during an outburst. Thus the apparent luminosity rise during an outburst is mainly caused by an increase of beaming. Because protons are co-accelerated with the electrons, our model predicts correlated variability of the synchrotron and high-energy SED component, with a possible lag of the high-energy hump caused by the longer acceleration and energy loss time scale of the protons in comparison to the electrons.

4 Predicted neutrino emission

4.1 Neutrino spectra

In contrast to leptonic models, in hadronic models γ -ray production by pion photoproduction would result in simultaneous neutrino production. The main neutrino production channel is through the decay of charged pions, e.g. $\pi^\pm \rightarrow \mu^\pm + \nu_\mu/\bar{\nu}_\mu$ followed by $\mu^\pm \rightarrow e^\pm + \nu_e/\bar{\nu}_e + \nu_\mu/\bar{\nu}_\mu$. The neutrinos escape without further interaction. Fig. 9 shows the predicted average neutrino emission from Mkn 421 and PKS 0716+714. The photon-hadron interactions for both, LBLs and HBLs, take place predominantly in the resonance region. Here, π^- and thus $\bar{\nu}_e$ production is suppressed. We give the predicted neutrino emission from the objects themselves, and do not consider here any additional contribution from escaping cosmic rays interacting while propagating through the cosmic microwave background radiation.

Provided Mkn 421 and PKS 0716+714 are typical for their respective object class, and that the Doppler factor in Mkn 421 is comparable or higher than in PKS 0716+714, we find a clear dominance of neutrino emission from LBLs in comparison to HBLs. The reason for this is the higher meson production rate in the LBL source population due to their higher target photon fields in comparison to the HBL population where proton synchrotron losses dominate. Thus more power, in our modeling for Mkn 421 by a factor of 10^3 – 10^4 , is channeled into the photon component in HBLs, while in LBLs the power output of photons and neutrinos is approximately equal. This is in contrast to previous hadronic jet models which predict equal photon and neutrino energy fluxes for all blazar types (e.g. [9]).

The neutrino production spectrum depends on the ambient proton spectrum and the spectrum and density of target photons. The proton injection spectrum is modified by interactions and energy losses. For Mkn 421 the photopion production rate approximately follows a broken power law, $t_\pi'^{-1} \propto \gamma_p'^{1.25}$ for proton energies below $\sim 10^7$ GeV, and $t_\pi'^{-1} \propto \gamma_p'^{0.5}$ above $E_p' \sim 10^7$ GeV due to the break in the target photon spectrum (see Fig. 1). This leads to a break in the neutrino spectrum at $\sim 10^7$ GeV (observer frame), from power spectral index $\alpha_\nu \approx 1.25$ to $\alpha_\nu \approx 0.5$ where $(E^2 dN/dE) \propto E^{\alpha_\nu}$. A further low energy break in the neutrino spectrum at $\sim 10^4$ GeV is caused by the change of photopion production rate at threshold. The high-energy cutoff at $\sim 10^9$ GeV in the observer's frame, caused by μ^\pm -synchrotron losses (π^\pm -synchrotron emission is unimportant), is below the strict upper limit of $E_\nu \leq 3 \times 10^{10}$ GeV predicted by [12]. Another important source

of high energy neutrinos is the production and decay of charged kaons when the proton-photon interaction takes place predominantly in the secondary resonance region of the cross section [16]. This might be the case for HBLs because their target photon field can extend up to X-ray energies. Positively charged kaons decay with $\sim 64\%$ probability into muons and direct high energy muon-neutrinos. These muon-neutrinos will not have energies reduced as a result of synchrotron radiation by their parent particles. Unlike the neutrinos originating from π^\pm and μ^\pm -decay, they will dominate the neutrino flavors at the high energy end of the emerging neutrino spectrum ($E_\nu > 10^9$ GeV), and also cause the total neutrino spectrum to extend to $\sim 10^{10}$ GeV.

We expect the neutrino emission from PKS 0716+714 to be cut off at $\sim 10^9$ GeV (observer frame) for all neutrino flavors (see Fig. 9) due to a roughly one order of magnitude lower proton cutoff. Also μ^\pm synchrotron losses may play a role here, and are expected to cut off at the same neutrino energy of $\sim 10^9$ GeV. The neutrino spectrum follows a power law with index $\alpha_\nu \approx 1.25$ below the cutoff, and is caused by photohadronic interactions with the target photon field above ϵ'_b . Because of the π -production threshold and the relatively low proton cutoff in LBLs, meson production in the photon field below ϵ'_b cannot occur.

In addition to the neutrinos from the meson decay chain, there will be a small contribution of $\bar{\nu}_e$ from neutron decay (not shown in the figures). For R' of 10^{15} to 10^{17} cm only neutrons of energy 30 to 3000 GeV will decay inside the production region. High-energy neutrons leaving the source into the observer's sight line will decay and produce highly beamed neutrinos, which also makes them appearing to come from the AGN. In addition, there will be also a contribution from neutrons decaying close enough to the system to appear a point source to the observer. The $\bar{\nu}_e$ flux from neutron decay at about 1 TeV will be approximately the same as the ν_e flux at that energy.

Neutrons produced during pion photoproduction interactions of protons may escape from the emission region if the optical depth for neutron-photon interactions, $\tau_{n\gamma}$, is less than one. In this optically thin case, the escaping neutrons may decay outside the AGN to become cosmic rays. Since the output of cosmic rays would then be related to the neutrino output, the observed cosmic ray intensity can be used to set an upper bound on the extragalactic neutrino background (ENB) due to neutrino emission by optically thin photoproduction sources [35, 36]. If, on the other hand, the source is optically thick to neutron-photon interactions the upper bound on the ENB intensity [36] is obtained instead from the observed diffuse gamma-ray background. We can determine which bound, optically thick or optically thin, should apply to LBLs and HBLs by considering the relevant time scales. The neutron-photon optical depth is $\tau_{n\gamma} = (R'/c)t'_{n\gamma}$. Note that since $t'_{\text{ad}} \approx R'/c$ (Appendix A) and that to a reasonable approximation $t'_{n\gamma} \approx t'_\pi$, we have $\tau_{n\gamma} \approx t'_{\text{ad}}/t'_\pi$. From Figs. 4a, 5a and 6a we see that for HBLs $\tau_{n\gamma} \ll 1$, and that for LBLs $\tau_{n\gamma} > 1$. Thus the optically thin bound should apply for HBLs and the optically thick bound for LBLs.

4.2 Diffuse neutrino fluxes

From Fig. 9 we expect that the contribution from LBLs to the diffuse extragalactic neutrino background (ENB) would dominate unless HBLs turn out to be significantly more numerous than LBLs. There are several methods to estimate the diffuse neutrino background. One method which has been suggested in [32] is to normalize to the observed extragalactic diffuse γ -ray background [33]. If LBLs dominate the blazar contribution of $\sim 25\%$ [34] to the extragalactic γ -ray background at GeV energies, then we would expect a diffuse integrated neutrino intensity of $\approx 10^{-7}$ GeV cm $^{-2}$ s $^{-1}$ sr $^{-1}$. However, HBLs may dominate the TeV-photon background, and by extrapolating the observed photon background to TeV-energies and normalizing the neutrino output from HBLs to the TeV-background, we would find a diffuse flux from HBLs of about 3–4 orders of magnitude lower. Taking this into account, the predicted ENB intensity from HBLs lies several orders of magnitude below the neutrino upper bounds [35, 36].

If the LBL and HBL luminosity function is known, the diffuse neutrino background is readily derived by convolving this luminosity function with the neutrino output of each source and integrating over redshift:

$$I_{\text{ENB}}(E) = \frac{1}{4\pi} \int dz \frac{dV_c}{dz} \frac{1+z}{4\pi d_L^2} \int dL^{\text{peak}} \rho(L^{\text{peak}}, z) I_\nu((E(1+z), L^{\text{peak}}))$$

where V_c is the co-moving cosmological volume, z is the redshift, d_L is the luminosity distance, and $\rho(L, z)$ is the source differential luminosity function at peak luminosity, $L^{\text{peak}} = \nu L_\nu^{\text{peak}}$ of the low energy hump of the SED. We have assumed no luminosity or density evolution for BL Lac Objects, in good agreement with the observations [37–39]. Note that the apparent negative evolution of HBLs found in early studies might be a selection effect [38]. For the LBL differential BL Lac luminosity function we used the 5 GHz luminosity function of Urry et al. [40] which we parametrize as

$$\rho(L_{5\text{GHz}}) = 10^{-33} \left\{ \left[\left(\frac{L_{5\text{GHz}}}{L^*} \right)^{-1.6} \right]^{-1} + \left[\left(\frac{L_{5\text{GHz}}}{L^*} \right)^{-3.3} \right]^{-1} \right\}^{-1} \text{ Gpc}^{-3} (\text{erg s}^{-1} \text{ Hz}^{-1})^{-1},$$

where $L^* = 2 \times 10^{33} \text{ erg s}^{-1} \text{ Hz}^{-1}$. We use $q_0 = 0$ and $H_0 = 50 \text{ km s}^{-1} \text{ Mpc}^{-1}$ as in [40]. The total radio BL Lac space density is estimated to be $\sim 1000 \text{ Gpc}^{-3}$ with the HBL contribution being about 10% of the LBL contribution, and so we used $N_{\text{HBL}}/N_{\text{LBL}} = 0.1$ in our calculation. Fig. 1 is used to convert the 5 GHz radio- to the synchrotron peak luminosity. For an LBL with νL_ν^{peak} at 1.3 eV (3.15×10^{14} Hz), such as in PKS 0716+714, and assuming that $\nu L_\nu \propto \nu^{0.5}$ for $\nu = 5$ GHz, then $\nu L_\nu^{\text{peak}}/\nu L_{5\text{GHz}} \approx 250$. The range of peak luminosities covered by the luminosity function is simulated by using different jet frame target photon densities, assuming that the directly accelerated e^- are responsible for the synchrotron hump and also represent the target photon field for $p\gamma$ -interactions and cascading. We keep all other parameters at the values derived for PKS 0716+714. A similar procedure is used for the HBLs where the parameters for calculating the ν -spectra

are derived from the fit to Mkn 421, and we used a range of target photon densities to simulate the luminosity range covered by the predicted luminosity function. For LBLs we used $u'_{\text{phot}} \approx 10^5 \dots 10^{12} \text{eV cm}^{-3}$, and for HBLs we have $u'_{\text{phot}} \approx 10^7 \dots 10^{12} \text{eV cm}^{-3}$. The cut-off energy of the injected proton spectrum is calculated self-consistently for each u'_{phot} value, and is mainly due to pion production losses for LBLs, and due to proton synchrotron losses for HBLs. The resulting diffuse neutrino fluxes are shown in Figs. 10a,b as the solid curves bounding the upper shaded region, where we have integrated over redshift up to $z = 3$. Also shown in these figures is the cosmic ray induced neutrino bound derived by [35, 36] for optically thick (Fig. 10a) and thin (Fig. 10b) sources and no source evolution.

Because $\nu L_{\nu}^{\text{peak}} \propto R'^2 D^4 u'_{\text{phot}}$, a range of synchrotron peak luminosities $\nu L_{\nu}^{\text{peak}}$ could instead arise due to different sizes of the emission volume for a constant jet frame target photon field u'_{phot} . To investigate how this would affect the ENB we have also calculated the contribution of LBLs to the diffuse neutrino flux in the following way. From the fits to the SED of PKS 0716+714 (Fig. 7b) we find a (jet frame) target photon energy density of $u'_{\text{phot}} \approx 10^{11} \text{eV cm}^{-3}$, corresponding to $\nu L_{\nu}^{\text{peak}} = 10^{47} \text{erg/s}$. For this $\nu L_{\nu}^{\text{peak}}$ -value we use the SED of PKS 0716+714 (Fig. 7b) and its associated neutrino output (Fig. 9) is used when calculating the contribution of LBLs with $\nu L_{\nu}^{\text{peak}} = 10^{47} \text{erg/s}$ to the ENB. For other $\nu L_{\nu}^{\text{peak}}$ -values, we assume the same target photon density $u'_{\text{phot}} \approx 10^{11} \text{eV cm}^{-3}$ but increase or decrease the emission region radius to give the desired $\nu L_{\nu}^{\text{peak}}$ -value, and calculate the neutrino output using the SPB model. The contribution of HBLs to the diffuse neutrino flux is calculated in a similar way, assuming that the number of HBLs is 10% of the number of LBLs [20], but this time using our fits to the SED of Mkn 421 (Fig. 7a), and its associated neutrino flux (Fig. 9) as a template for all HBLs with $\nu L_{\nu}^{\text{peak}} = 8 \times 10^{42} \text{erg/s}$ and $u'_{\text{phot}} \approx 10^{10} \text{eV cm}^{-3}$. For different $L_{5\text{GHz}}$ -values we again increase or decrease the emission region radius to give the desired $\nu L_{\nu}^{\text{peak}}$ -value keeping $u'_{\text{phot}} \approx 10^{10} \text{eV cm}^{-3}$. The upper dashed curves in Figs. 10a,b show the resulting neutrino fluxes. In reality, the synchrotron luminosity may vary simultaneously due to both a varying intrinsic synchrotron photon density and a varying emission volume. The (upper) shaded area therefore gives the uncertainty in our calculation assuming that the luminosity conversion ratio $\nu L_{\nu}^{\text{peak}}/L_{5\text{GHz}}$ we have adopted (based on our “average” SEDs) and used to convert the 5 GHz luminosity function into a 1.3 eV luminosity function is correct.

Our estimated diffuse neutrino flux depends strongly on the $L_{\nu}^{\text{peak}}/L_{5\text{GHz}}$ -ratio, which in turn is rather uncertain. To show this, we have repeated the calculation for an LBL with a luminosity peak at lower frequency, e.g. PKS 0537-441. Here one finds $\nu L_{\nu}^{\text{peak}}/\nu L_{5\text{GHz}} \approx 60$ for $\nu^{\text{peak}} \approx 0.07 \text{eV}$. The lower shaded area shows the resulting estimates of the diffuse neutrino flux.

The discussion above shows that there is a large uncertainty in our predicted diffuse neutrino flux, with ~ 3 orders of magnitude alone due to the uncertainty in the $\nu L_{\nu}^{\text{peak}}/\nu L_{5\text{GHz}}$ ratio, in addition to the uncertain BL Lac luminosity function and its LBL fraction.

5 Summary and Discussion

We have presented a parameter study of the SPB model proposed recently to explain the observed spectral energy distribution of γ -ray loud BL Lac Objects, i.e. HBLs and LBLs. This model needs strong magnetic fields together with proton, muon and pion synchrotron radiation in order to produce the double-humped structure observed during active phases of γ -ray emission, and this is the main difference to the original hadronic “proton initiated cascade” (PIC) model [8, 9] which resulted in a rather featureless $\pi^{0,\pm}$ -cascade spectrum.

If LBLs possess denser jet frame synchrotron photon fields than HBLs, i.e. denser target photon fields for $p\gamma$ interactions and cascading in our model, then we have shown that the high-energy emission in these two types of objects is of different origin. While the MeV-TeV radiation from HBLs is dominated by proton synchrotron radiation, in LBLs there is a significant contribution from muon synchrotron radiation at GeV-TeV energies in addition to the proton synchrotron radiation which dominates at MeV-energies. This is caused by the significantly higher pion (and muon) production rate. Consequently the injected proton spectrum is cut off due to pion production losses in LBL-like objects, while in HBL-like objects proton synchrotron radiation is responsible for the cut off in the proton spectrum. These cutoffs directly translate into the observed high energy photon cutoff at the source if the Doppler factor is known.

A further consequence of different intrinsic target photon fields in HBLs and LBLs is a difference in the ratio of the luminosity in the high energy hump to low energy hump in their cascade spectra (due to proton acceleration). Because opacity effects decisively influence this ratio, the cascade spectra of LBLs have in general smaller ratios than that of HBLs. Also, the high energy peak to “dip” luminosity appears to be smaller in the denser LBL-like environments than in HBLs. This is a consequence of the higher pion production rate in LBLs in comparison to HBLs which causes the featureless π -cascade to become important and fill in the gap between the two humps with proton and muon radiation.

To demonstrate the difference between LBLs and HBLs in the SPB-model we have fitted the average observed SED of PKS 0716+714 and Mkn 421. In doing so, we found that HBLs need acceleration efficiencies of order unity to give high energy hump energies in the TeV-range, whereas for LBLs acceleration efficiencies of $\sim 10^{-2}$ seem to account for the observations. LBLs may also produce multi-TeV photons at a lower level than HBLs despite their higher bolometric luminosity. The production mechanism is through muon synchrotron radiation that peaks at a higher energy than the synchrotron radiation of the primary protons. We therefore suggest that nearby LBLs be included in the observing source lists of future high-sensitivity Cherenkov-telescopes (see, e.g., [41]).

Gamma-ray loud BL Lacs are well-known for their flaring activity, and we have modeled the nearly simultaneous observations of the intermediate and flaring stage of the famous 1997 giant outburst of Mkn 501. An increase of the Doppler factor and acceleration efficiency, together with rising proton and electron density (leading to a denser intrinsic synchrotron target photon field) can account for the observations satisfactorily.

Because the observations were only simultaneous on a one-day time scale at most we believe that our time-independent code is suitable for this simulation. At this point we stress the need for time-resolved simultaneous observations to provide further constraints for blazar modeling, which then must be carried out using time-dependent simulation codes.

Although proton and muon synchrotron emission, and their reprocessed radiation, produce a double-humped structure in typical blazar jet environments, namely one at X-ray energies, and another at GeV-TeV energies, the low-energy synchrotron target photon field dominates over the X-ray hump in the cascade spectrum in nearly all cases presented here. This seems to suggest that the SS-PIC model proposed by [25,42], where the observed X-ray hump is due to reprocessed proton and muon synchrotron radiation, is constrained to a rather narrow parameter range, and this is shown in [42]. The relatively small Doppler factors favoured in [42] imply thick target photon fields, and consequently significant reprocessing leading to comparable power at X-ray and sub-TeV energies but making it difficult to explain the high-energy bump to be at multi-TeV energies.

The dominance of proton synchrotron radiation in HBLs has recently been used by [26] to consider a blazar model where all proton synchrotron photons escape the completely optically thin emission region, and appear as the high-energy hump in the blazar SED. This occurs in intrinsically thin or extremely low energetic ambient photon fields (i.e. very high Doppler factors $D \approx 10\text{--}30$ are necessary), where $p\gamma$ -interactions and cascading can be neglected, and extremely large magnetic fields of ~ 100 G are necessary to fit the observed SED in this case. If the X-ray emission is produced by synchrotron emission in the strong magnetic field from secondary electrons which are the result of $\gamma\gamma$ -pair production of the TeV synchrotron photons of the primary protons with an ambient external infrared photon field, then the X-ray flare is expected to lag the γ -ray flare. Since acceleration of electrons is faster than of protons, $t'_{\text{acc,p}} \gg t'_{\text{acc,e}} \approx t'_{\text{syn,e}}$, typically by a few hours for blazars, γ -rays should lag X-rays if the X-rays stem from the primary co-accelerated electrons.

If electrons are accelerated in the same process as the protons, γ -rays from the PIC-processes are in competition with photons from the leptonic SSC process. SSC-photons contribute significantly to the escaping radiation if $u'_B \ll u'_{\text{phot}}$, i.e. $u'_{\text{phot}} > 10^{13}\text{eV cm}^{-3}(B'/30\text{G})^2$. So far, all known γ -ray loud BL Lac objects have an energy density low-frequency hump $u'_{\text{phot}} < 10^{12}\text{eV cm}^{-3}$ for reasonable Doppler factors ($D \approx 10$) and emission volumes, $R^3 \approx (10^{15-17})^3 \text{ cm}^3$. We conclude that SSC emission is negligible in HBLs and LBLs if relativistic protons are the main carrier of the dissipated energy in a highly magnetized jet.

To calculate the total jet luminosity L_{jet} measured in the rest frame of the galaxy we follow the procedure given in [43]. Under the assumption that all particles (electrons and protons) are relativistic one obtains

$$L_{\text{jet}} = 4p'_p \Gamma^2 \beta c \pi R'^2 \left[\chi_p \frac{(\Gamma - 1)}{\Gamma} + 1 + \frac{p'_B}{p'_p} + \frac{p'_e}{p'_p} \right] \quad (3)$$

$$= \frac{L_{\text{obs}}^{\text{high}}}{D^4 \zeta_p} \left[\chi_p \frac{(\Gamma - 1)}{\Gamma} + 1 + \frac{p'_B}{p'_p} + \frac{\zeta_p L_{\text{obs}}^{\text{low}}}{\zeta_e L_{\text{obs}}^{\text{high}}} \right] \quad (4)$$

where $\Gamma = (1 - \beta^2)^{-1} \approx D/2$ is a good approximation to the Lorentz factor of jets closely aligned to the line of sight. $L_{\text{obs}}^{\text{low}}$ and $L_{\text{obs}}^{\text{high}}$ are the observed bolometric luminosities of the low and high energy component, respectively, and $\zeta_e \approx 1$, ζ_p are the radiative efficiencies for electrons and protons. $u'_B = 3p'_B$ is the magnetic energy density of a tangled magnetic field and

$$p'_p = \frac{L_{\text{obs}}^{\text{high}}}{4D^4 \zeta_p \Gamma^2 \beta c \pi R'^2} \quad (5)$$

$$p'_e = \frac{L_{\text{obs}}^{\text{low}}}{4D^4 \zeta_e \Gamma^2 \beta c \pi R'^2} \quad (6)$$

gives the jet-frame pressure of injected relativistic protons and electrons, respectively, that would apply in the absence of energy loss mechanisms, and

$$\chi_p = \frac{3}{4} \left(\frac{p'_e}{p'_p} \frac{1}{\gamma'_{e1} \ln(\gamma'_{e2}/\gamma'_{e1})} + \frac{1}{\gamma'_{p1} \ln(\gamma'_{p2}/\gamma'_{p1})} \right) \quad (7)$$

$$= \frac{3}{4} \left(\frac{\zeta_p S_{\text{obs}}^{\text{low}}}{\zeta_e S_{\text{obs}}^{\text{high}}} \frac{1}{\gamma'_{e1} \ln(\gamma'_{e2}/\gamma'_{e1})} + \frac{1}{\gamma'_{p1} \ln(\gamma'_{p2}/\gamma'_{p1})} \right). \quad (8)$$

(Note the erroneous Eq.28+29 in [11].) Here $\gamma'_{e1}, \gamma'_{e2}$ are the lower and upper limit of the injected electron spectrum, respectively. The ratio of the number of electrons to protons on injection is then

$$\frac{n'_e}{n'_p} = \frac{p'_e m_p \gamma'_{p1} \ln(\gamma'_{p2}/\gamma'_{p1})}{p'_p m_e \gamma'_{e1} \ln(\gamma'_{e2}/\gamma'_{e1})}. \quad (9)$$

The resulting jet power for HBLs typically lie around 10^{45} erg/s, for LBLs typically 10^{47} erg/s, higher than in leptonic SSC models but consistent with estimated upper limits for BL Lacs [44]. Injected n'_e/n'_p -ratios are typically $10^{-3} - 1$ for HBLs and approximately unity for LBLs assuming $\gamma'_{e1} = 2$, i.e. most relativistic electrons responsible for the low-energy hump in the SED would be primaries, co-accelerated with the protons. The addition of cold electrons possibly needed for charge neutrality in HBLs if $n'_e/n'_p < 1$ would add little to the estimated jet power.

A caveat in hadronic models is that most processes are rather slow in comparison to leptonic interactions. Indeed, if pion production dominates the loss processes, variability time scales below $t_{\text{var}} \approx 10^3(10/D)(30 \text{ G}/B')^2$ s at the highest photon energies would not be expected. This limit is based on $u'_B = u'_{\text{phot}}$ and $\eta = 1$, and assuming that the size of the emission region does not constrain the variability time scale. For HBLs proton synchrotron radiation dominates the loss processes. Hence, the smallest variability time scale (again provided R' does not determine t_{var}) depends on the Doppler factor, magnetic field and η , which in turn determines essentially the high energy photon turnover ϵ_{TeV} (in TeV): $t_{\text{var}} \approx 10^4[(D/10)\epsilon_{\text{TeV}}(B'/30 \text{ G})]^{-0.5}$ sec with $\epsilon_{\text{TeV}} \leq 1.1(D/10) \text{ TeV}$ corresponding

to $\eta \leq 1$. Thus, for extremely high magnetic fields and/or Doppler factors variability on sub-hour time scales can be reached.

The basic difference between the leptonic SSC model and our presented hadronic model is the content of the jet: while leptonic models work with a relativistic electron/positron plasma, our model considers a relativistic electron/proton jet. For fitting the observed SEDs leptonic models need significantly smaller magnetic field values (e.g. $B' = 0.497$ G [24] or 0.8 G [31] for Mkn 501, $B' = 0.46$ G for PKS 0716+714 and $B' = 0.093$ G for Mkn 421 [24]) while the size of the emission region and Doppler factor are comparable to the values used in this model (e.g. [24] gives $R' = 10^{16}$ cm for Mkn 501 and Mkn 421, and $R' = 5 \times 10^{16}$ cm for PKS 0716+714, $D=10, 12$ and 15 for Mkn 501, Mkn 421 and PKS 0716+714, respectively, [31] gives $R' = 5 \times 10^{15}$ cm and $D = 15$ for the flaring state of Mkn 501). As a consequence, in leptonic models the particle energy density is often significantly higher than the magnetic field energy density.

If the magnetic field component along the line of sight is much stronger in hadronic models than in leptonic ones, the rotation measure RM on a length scale of the emission region ($\sim 10^{15}$ cm) may provide a tool to distinguish between the competing models. Observations of spatial and temporal variability of the RM in the central parsecs of AGN suggest that the measured RM is indeed intrinsic to the source and no foreground effect (e.g. [48]). The observed Faraday rotation may therefore serve as a probe of the magnetic field weighted by the electron density in the so-called Faraday screen along the line of sight on the observed length scale. In radio galaxies and quasars the Faraday screen is often considered to be the narrow (NLR) or broad line region (BLR) (e.g. [49], [48]), and electron densities are derived from the NLR/BLR optical line strengths. According to the unified scheme the proposed picture for BL Lac Objects consists of a relativistic jet that evacuates a cone through the ionized gas in the nuclear region such that cores of BL Lacs are not viewed through a dense Faraday screen, and lower RM -values are therefore expected from BL Lac Objects (e.g. [49]). To date, RM measurements from AGN exist only on kpc-pc scales. E.g., for BL Lacs [50] recently found $RM \sim$ several 100 rad m⁻² on 1-50pc scales. Assuming $N_e \approx 10 - 100$ cm⁻³ these values fit to the strong magnetic fields in hadronic models if the field decays along the jet as $R^{-1.5 \dots -2}$. High-resolution RM observations on the central 10^{-3} pc scales and a definite identification of the Faraday screen in BL Lacs are needed to clearly constrain the magnetic field in the gamma ray emission region.

In contrast to leptonic models, models involving pion production inevitably predict neutrino emission due to the decay of charged mesons. In the present work, we predict the neutrino output of a typical LBL, PKS 0716+714, and a typical HBL, Mkn 421. If LBLs possess intrinsically denser target photon fields than HBLs, then within the SPB model, higher meson production rates are expected in LBLs, leading to a higher neutrino production rate. The diffuse neutrino background will therefore be dominated by LBLs, unless HBLs turn out to be significantly more numerous than LBLs.

To estimate the diffuse neutrino flux we must know the luminosity functions of HBLs and LBLs, and the neutrino energy spectrum of HBLs and LBLs as a function of their

luminosity. Because of the uncertainties in the BL Lac luminosity function and the conversion from low energy peak to 5 GHz-luminosity, the diffuse neutrino flux can only be predicted within a large uncertainty of more than three orders of magnitude. To reduce this uncertainty, it would be helpful to have a luminosity function for νL_ν^{peak} or the bolometric luminosity of the low-energy hump.

Acknowledgements

We thank Alina Donea for helpful discussion. The research of RJP is supported by the Australian Research Council. RE and TS are supported in part by NASA Grant NAG5-7009 and by the US Department of Energy contract DE-FG02 91ER 40626. AM has been supported by the Quebec Government by a postdoctoral bursary, and thanks the Bundesministerium für Bildung und Forschung for financial support through DESY grant Verbundforschung 05CH1PCA6. The work of JPR has been supported by the EU-TMR network Astro-Plasma-Physics (ERBFMRX-CT98-0168).

References

- [1] C.D. Dermer & R. Schlickeiser, *ApJ* **416** (1993), 458.
- [2] M. Böttcher, H. Mause & R. Schlickeiser, *A&A* **324** (1997), 395.
- [3] M. Sikora, M.C. Begelman & M.J. Rees, *ApJ* **421** (1994), 153.
- [4] M. Blazejowski, M. Sikora, R. Moderski & G.M. Madejski, *ApJ* **545** (2000), 107.
- [5] A.-C. Donea and R.J. Protheroe, *Astropart.Phys.*, submitted
- [6] L. Maraschi, G. Ghisellini & A. Celotti, *ApJ* **397** (1992), L5.
- [7] S.D. Bloom & A.P. Marscher, *ApJ* **461** (1996), 657.
- [8] K. Mannheim & P.L. Biermann, *A&A* **221** (1989), 211.
- [9] K. Mannheim, *A&A* **269** (1993), 67.
- [10] A. Mücke & R.J. Protheroe, *Proc. workshop "GeV-TeV Astrophysics: Toward a Major Atmospheric Cherenkov Telescope VI"*, *AIP Conf. Proc.* Vol 515 (2000), 149, eds.: B.D. Dingus et al.
- [11] A. Mücke & R.J. Protheroe, *Astropart. Phys* **15** (2001), 121.
- [12] J. Rachen & P. Mészáros, *Phys. Rev D* **58** (1998), 123005.

- [13] R.J. Protheroe, *Proc. IAU Colloq. 163*, Accretion Phenomena and Related Outflows, ed. D. Wickramasinghe et al. (1996).
- [14] J. Learned & K. Mannheim, *Ann.Rev.Nucl.Part.Sci.* **50** (2000), 679.
- [15] R.J. Protheroe & P. Johnson, *Astropart.Phys.* **4** (1996), 253, & erratum **5** (1996), 215.
- [16] A. Mücke et al., *Comm.Phys.Comp.* **124** (2000), 290.
- [17] R.J. Protheroe, *PASA*, submitted.
- [18] M. Pohl & R. Schlickeiser, *A&A* **354** (2000), 395.
- [19] R.D. Blandford & R.L. Znajek, *MNRAS* **179** (1977), 433.
- [20] P. Padovani & P. Giommi, *ApJ* **444** (1995), 567 (PG95).
- [21] E. Perlman, P. Padovani, P. Giommi, R. Sambruna, L.R. Jones, A. Tzioumis, J. Reynolds, *AJ* **115** (1998), 1253.
- [22] S.A. Laurant-Muehleisen, R.I. Kollgaard, E.D. Feigelson, W. Brinkmann, J. Siebert, 1998, *ApJS* **525** (1999), 127.
- [23] A. Caccianiga, T. Maccacaro, A. Wolter, R. Della Ceca, I.M. Gioia, *ApJ* **513** (1999), 51.
- [24] G. Ghisellini et al., *MNRAS* **301** (1998), 451.
- [25] J.P. Rachen 1999, in: Proc. of “GeV-TeV Astrophysics: Toward a Major Atmospheric Cherenkov Telescope V”, Snowbird, Utah (August, 1999).
- [26] F.A. Aharonian, *New Astron.* **5** (2000), 377.
- [27] W. Bednarek & R.J. Protheroe, *MNRAS* **310** (1999), 577.
- [28] G. Henri, G. Pelletier, P.O. Petrucci, N. Renaud, *Astropart. Phys.* **11** (1999), 347.
- [29] C.A. Haswell, T. Tajima, J.J. Sakai, *ApJ* **401** (1992), 495.
- [30] N. Gehrels & P. Michelson, *Astropart. Phys.* **11** (1999), 277.
- [31] E. Pian et al., *ApJ* **492** (1998), L17.
- [32] A. Mücke & R.J. Protheroe, Proc. 27th Int. Cosmic Ray Conf., Hamburg/Germany, **Vol. 3**, (2001), 1153.
- [33] P. Sreekumar et al., *ApJ* **494** (1998), 523.

- [34] J. Chiang & R. Mukherjee, *ApJ* **496** (1998), 752.
- [35] E. Waxman & J. Bahcall, *Phys. Rev. D* **59** (1999), 023002.
- [36] K. Mannheim, R.J. Protheroe & J.P. Rachen, *Phys Rev D* **63** (2001), 023003.
- [37] P. Padovani, *Proc. workshop "Blazar Demographics and Physics"*, *ASP Conf. Series* **227** (2001), eds.: P. Padovani & C.M. Urry.
- [38] P. Giommi & A. Pellizzoni, *Proc. workshop "Blazar Demographics and Physics"*, *ASP Conf. Series* **227** (2001), eds.: P. Padovani & C.M. Urry.
- [39] A. Caccianiga, T. Maccacaro, A. Wolter, R. Della Ceca, I.M. Gioia, *ApJ* **566** (2002), 181.
- [40] C.M. Urry, P. Padovani & M. Stickel, *ApJ* **382** (1991), 501.
- [41] F. Krennrich, in: "TeV gamma-ray astronomy in the New Millennium", 7th Taipei Astrophysics Workshop on Cosmic Rays in the Universe, Ed. C.-M. Ko, ASP Conference Series, Vol. 241 (2001), 141.
- [42] J. Rachen, in: "*Gamma-2000*", Heidelberg, AIP Proceedings, eds.: F.A. Aharonian & H.J. Völk, **558** (2000), 704.
- [43] R.J. Protheroe and A.-C. Donea, to be submitted.
- [44] A. Celotti, P. Padovani, G. Ghisellini, *MNRAS* **286** (1997), 415.
- [45] A.D. Kerrick et al., *ApJ* **452** (1995), 588.
- [46] F.W. Stecker & M.H. Salamon, *Space Sci.Rev.* **75** (1996), 341.
- [47] L. Nellen, K. Mannheim & P.L. Biermann, *Phys.Rev.D* **47** (1993), 5270.
- [48] R.T. Zavala & G.B. Taylor, *American Astronomical Society Meeting* **199** (2001).
- [49] G.B. Taylor, *ApJ* **533** (2000), 95.
- [50] R.T. Zavala & G.B. Taylor, *American Astronomical Society Meeting* **200** (2002).

A Energy losses from adiabatic jet expansion

The rate of proton energy change due to adiabatic jet expansion/contraction is given by

$$\left(\frac{dE}{dt}\right)'_{\text{ad}} = -\frac{E'}{3} \vec{\nabla} \cdot \vec{v}$$

where \vec{v} is the flow velocity. We consider a velocity field within the jet which is directed radially outward. On the jet axis at a distance z from the central engine we can approximate:

$$\vec{\nabla} \cdot \vec{v} \approx 2 \frac{v}{R'} \frac{dR'}{dz} + \frac{dv}{dz}$$

with $R'(z)$ the jet radius at distance z in the jet frame. Thus for a constant speed conical jet $\vec{v} = v\hat{r}$ with opening angle Θ (i.e. $R' \approx \Theta z$), we find:

$$\left(\frac{dE}{dt} \right)'_{\text{ad}} = -\frac{2v}{3z} E'$$

with $v = c\sqrt{1 - \gamma^{-2}}$ and $dv/dz = c^2/(\gamma^3 v)(d\gamma/dz) \approx c/\gamma^3(d\gamma/dz)$ for a relativistic jet. We obtain for the adiabatic loss time scale in the jet frame

$$t'_{\text{ad}} = \frac{3}{2} \frac{z}{\gamma c} \approx \frac{R'}{c}.$$

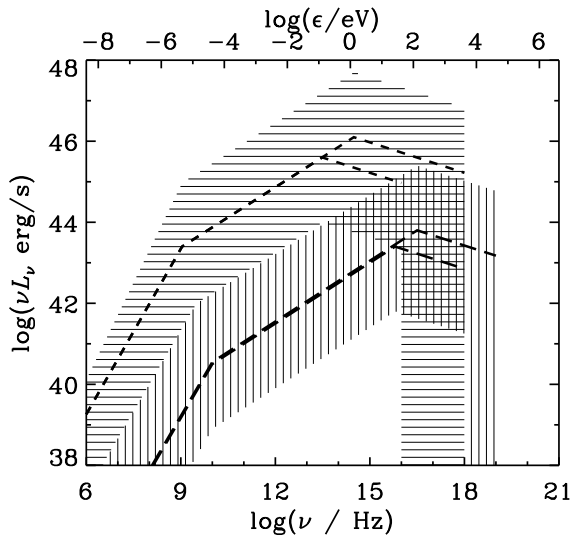


Figure 1: Form of the SED assumed for the synchrotron radiation from LBLs (short dashed curves) and HBLs (long dashed curves). The horizontal shading encompasses the SEDs of all LBLs, and the vertical shading encompasses the SEDs of all HBLs considered by [24].

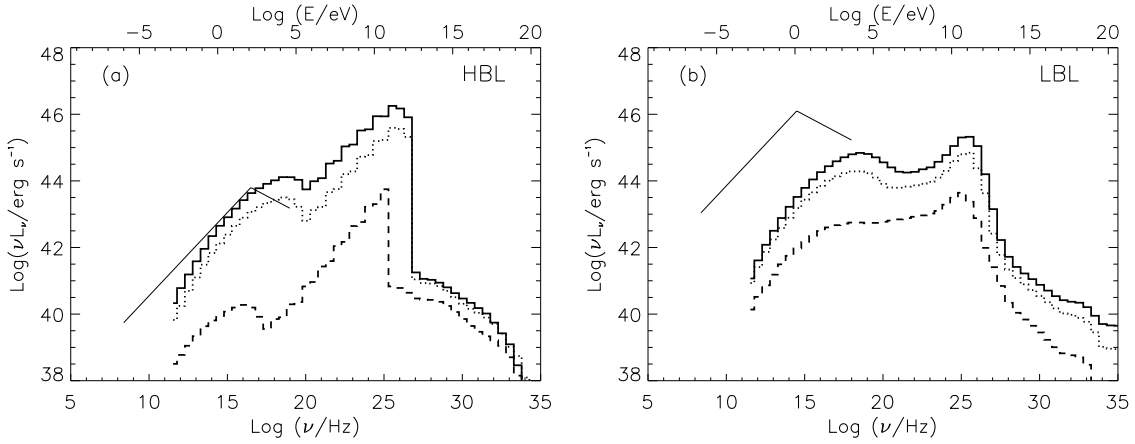


Figure 2: SED of emerging cascade radiation in the SPB model with target photon spectra (broken power-law) given by the synchrotron component of the “average” SED in Fig. 1: (a) HBLs with $\nu L_{\text{max, syn}} = 10^{43.8}$ erg/s, and (b) LBLs $\nu L_{\text{max, syn}} = 10^{46.1}$ erg/s, for $D = 8$, $R' = 5 \times 10^{15}$ cm and $B' = 10$ G (dashed histogram), 30 G (dotted histogram), 50 G (solid histogram). We assume equipartition between relativistic proton energy density and magnetic energy density $u'_B = u'_P$, and this gives $L_{\text{jet}}/10^{44}$ erg/s $\approx 4, 35, 98$ for HBLs and LBLs for the three magnetic fields (see Sect. 5 for the calculation of L_{jet}).

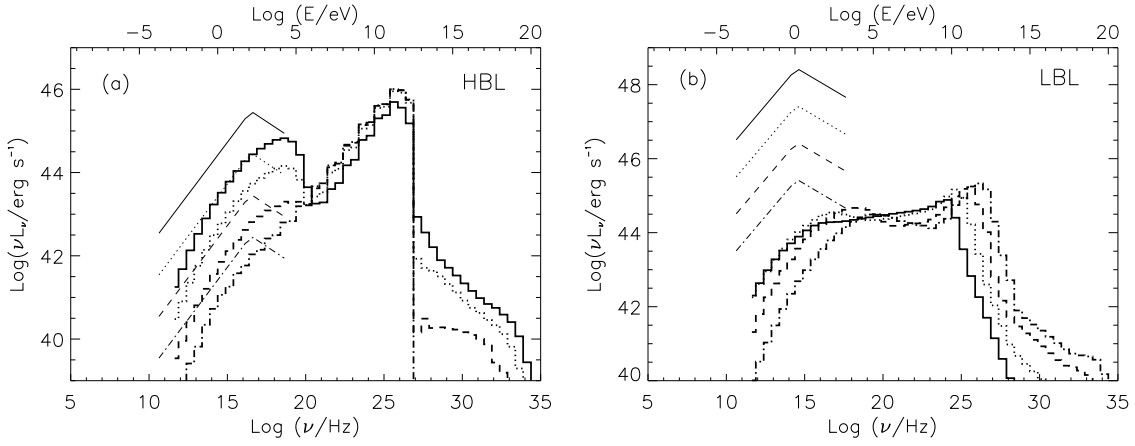


Figure 3: SED of emerging cascade radiation for different target photon spectra (broken power-laws shown), $u'_B = u'_P$, $B' = 30G$, $D = 10$, and $R' = 5 \times 10^{15}$ cm. (a) HBL-like synchrotron spectra with $u'_B = u'_P$, $\log(u'_{\text{phot}}/\text{eVcm}^{-3}) = 8, 9, 10, 11$ and $L_{\text{jet}}/10^{44}$ erg/s ≈ 55 for all $\log(\nu L_{\text{max,syn}}/\text{ergs}^{-1}) = 42.4, 43.4, 44.4, 45.4$. (b) LBL-like synchrotron spectra with $\log(u'_{\text{phot}}/\text{eVcm}^{-3}) = 11, 12, 13, 14$ and $L_{\text{jet}}/10^{45}$ erg/s $\approx 55, 55, 56, 58$ corresponding to $\log(\nu L_{\text{max,syn}}/\text{ergs}^{-1}) = 45.4, 46.4, 47.4, 48.4$.

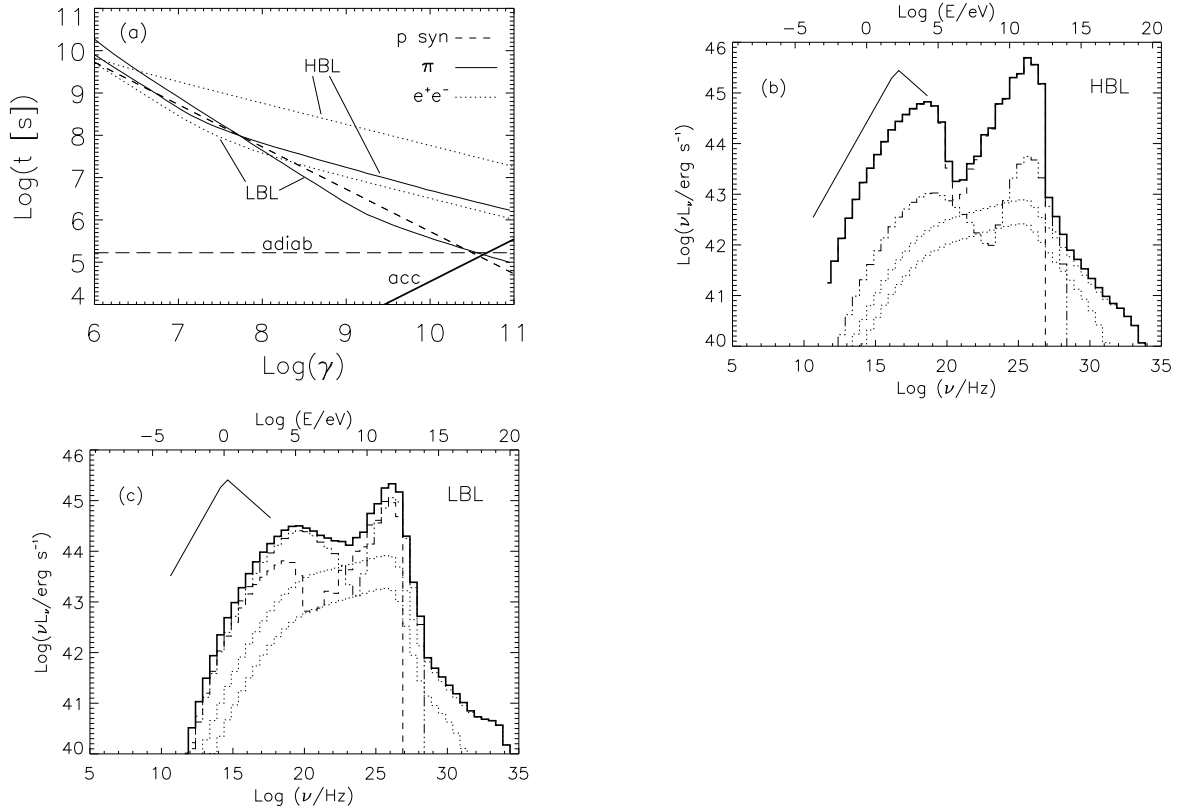


Figure 4: (a) Mean energy loss time (jet frame) of p in HBL-like and LBL-like target photon spectra for π -photoproduction (π), Bethe-Heitler pair production (e^+e^-) and proton synchrotron radiation (p syn) for $B' = 30G$, $\log(u'_{\text{phot}}/\text{eVcm}^{-3}) = 11$, $D = 10$, $R' = 5 \times 10^{15}$ cm, $u'_B = u'_p$. The acceleration time scale (acc) is indicated as a thick straight line. (b) SED of emerging cascade radiation for HBL-like synchrotron spectra. (c) SED of emerging cascade radiation for LBL-like synchrotron spectra. The target photon spectra are shown as a broken power-law curves on the left in each figure. Emerging cascade spectra: p synchrotron cascade (dashed line), μ synchrotron cascade (dashed-triple dot), π^0 cascade (upper dotted line) and π^\pm -cascade (lower dotted line).

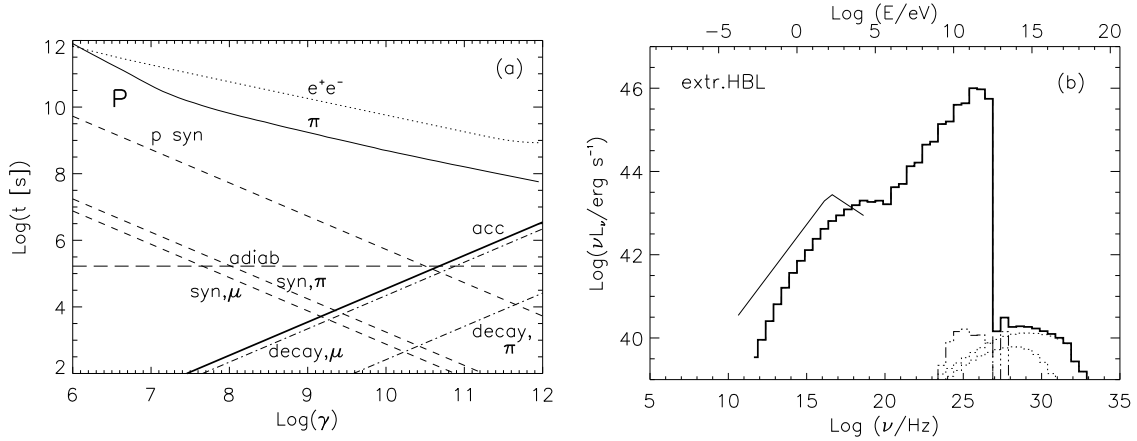


Figure 5: Example of an extreme HBL. Parameters: $B' = 30$ G, $D = 10$, $R' = 5 \times 10^{15}$ cm, $u'_{\text{phot}} = 10^9$ eV cm $^{-3}$, $\nu L_{\text{max,syn}} = 10^{43.4}$ erg/s, $L_{\text{jet}} \approx 5 \times 10^{45}$ erg/s, $u'_B = u'_P$, $\gamma'_{P,\text{max}} = 4 \times 10^{10}$. (a) Mean energy loss time (jet frame) of p for π -photoproduction (π), Bethe-Heitler pair production (e^+e^-) and synchrotron radiation (syn). Loss times for π^\pm and μ^\pm for synchrotron radiation (syn π , syn μ) are also shown and compared with their mean decay time scales (decay π , decay μ). The acceleration time scale (acc) is indicated as a thick straight line. (b) Emerging cascade spectra: p synchrotron cascade (dashed line), μ synchrotron cascade (dashed-triple dot), π^0 cascade (upper dotted line) and π^\pm -cascade (lower dotted line).

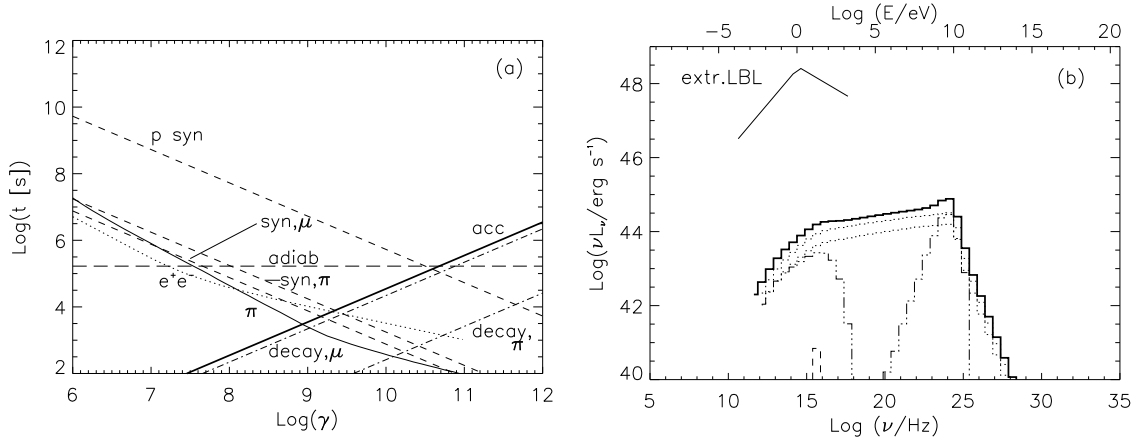


Figure 6: Example of an extreme LBL: Parameters: $B' = 30 \text{ G}$, $D = 10$, $R' = 5 \times 10^{15} \text{ cm}$, $u'_{\text{phot}} = 10^{14} \text{ eV cm}^{-3}$, $\nu L_{\text{max,syn}} = 10^{48.4} \text{ erg/s}$, $u'_B = u'_P$, $\gamma'_{P,\text{max}} = 8 \times 10^8$, $L_{\text{jet}} \approx 6 \times 10^{45} \text{ erg/s}$. (a) Mean energy loss time (jet frame) of p for π -photoproduction (π), Bethe-Heitler pair production (e^+e^-) and synchrotron radiation (syn). Loss times for π^\pm - and μ^\pm for synchrotron radiation (syn π , syn μ) are also shown and compared with their mean decay time scales (decay π , decay μ). The acceleration time scale (acc) is indicated as a thick straight line. (b) Emerging cascade spectra: p synchrotron cascade (dashed line), μ synchrotron cascade (dashed-triple dot), π^0 cascade (upper dotted line) and π^\pm -cascade (lower dotted line).

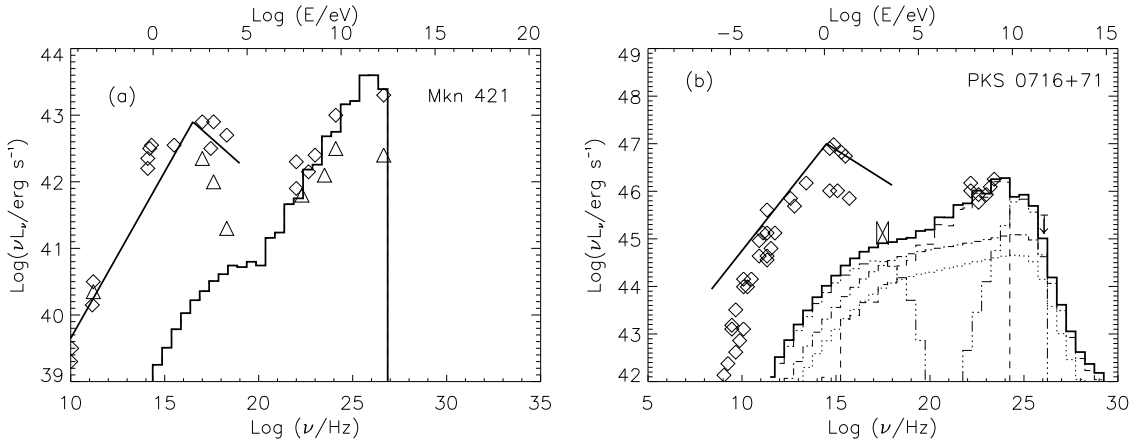


Figure 7: Modeling the SED of (a) Mkn 421 and (b) PKS 0716+714. The Mkn 421 data are corrected for pair production on the cosmic background radiation field [27], and represent the emitted spectrum at the source. The target photon distribution is indicated as a broken power law on the left side in each figure. Dotted line represents the π^0 -component, dashed-dotted line the π^\pm -component, dashed-triple dot the μ synchrotron, dashed line the p synchrotron component, and the solid line is the sum of all cascade components. Model parameters are: (a) $B'=30$ G, $D = 10$, $R' = 3 \times 10^{15}$ cm, $u'_{\text{phot}} = 10^9$ eV cm $^{-3}$, $u'_p \approx 1$ erg/cm 3 , $\gamma'_{p,\text{max}} = 4 \times 10^{10}$, $L_{\text{jet}} \approx 9 \times 10^{44}$ erg/s, $\eta = 1$. (b) $B' = 30$ G, $D \approx 7$, $R' \approx 10^{17}$ cm, $u'_{\text{phot}} \approx 10^{11}$ eV cm $^{-3}$, $u'_p \approx 6$ erg/cm 3 , $\gamma'_{p,\text{max}} = 3 \times 10^9$, $L_{\text{jet}} \approx 3 \times 10^{47}$ erg/s, $\eta = 0.01$. The 3σ upper limit is from 1994-Whipple observations [45]. Note that the absorption effects in the cosmic background radiation field are not taken into account here because of the uncertain redshift of PKS 0716+714.

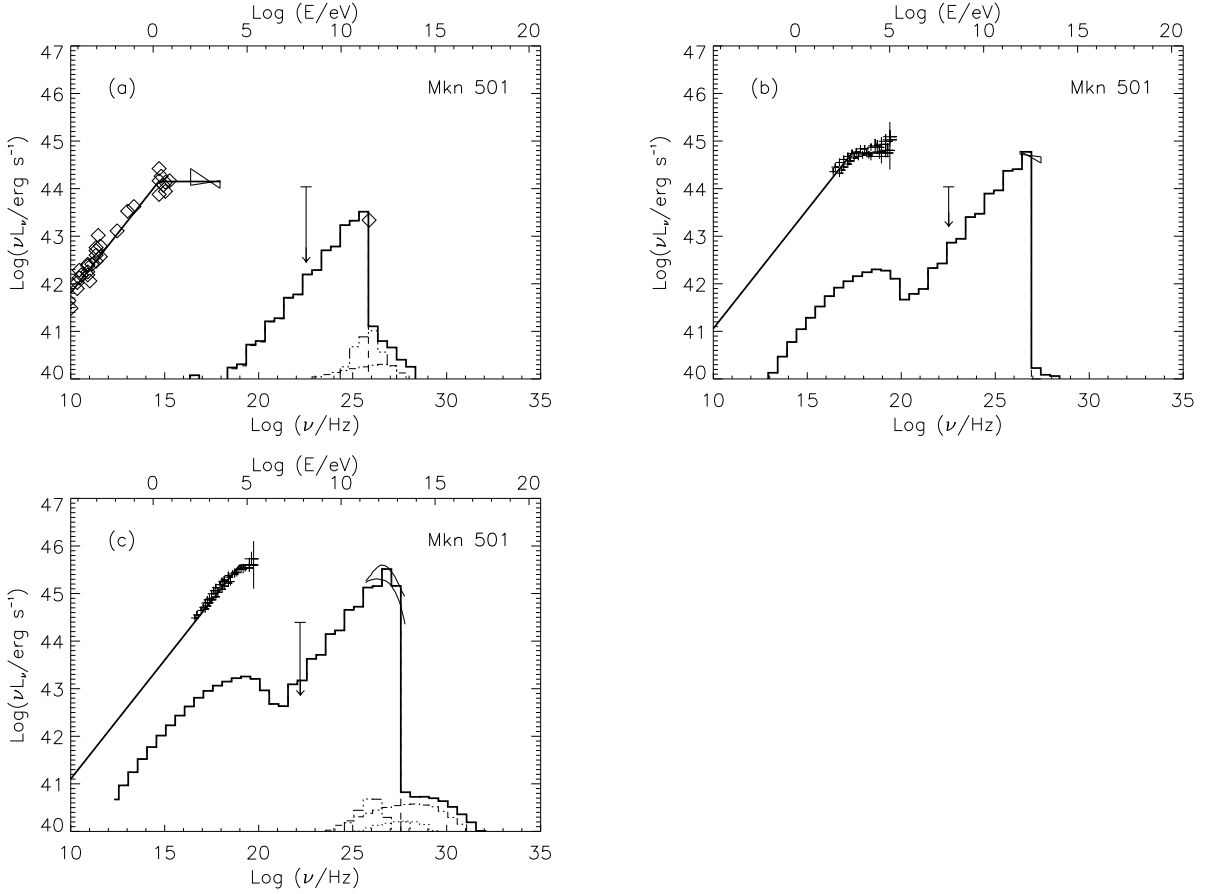


Figure 8: Modeling the SED of Mkn 501 in different activity states: (a) quiet state , (b) intermediate state and (c) outburst. The data are corrected for pair production on the cosmic background radiation field [27]. Dotted line represents the π^0 -component, dashed-dotted line the π^\pm -component, dashed-triple dot the μ synchrotron, dashed line the p synchrotron component, and the solid line is the sum of all cascade components. Model parameters are: a) $B' \approx 20$ G, $D = 9$, $R' \approx 5 \times 10^{15}$ cm, $u'_{\text{phot}} = 7 \times 10^9$ eV cm $^{-3}$, $u'_P = 0.8$ erg/cm 3 , $\gamma'_{P,\text{max}} = 10^{10}$, $e/p=1.3$, $L_{\text{jet}} \approx 1.4 \times 10^{45}$ erg/s, $\eta = 0.05$. b) $B' \approx 20$ G, $D = 11$, $R' \approx 5 \times 10^{15}$ cm, $u'_{\text{phot}} = 10^{10}$ eV cm $^{-3}$, $u'_P = 1.7$ erg/cm 3 , $\gamma'_{P,\text{max}} = 4 \times 10^{10}$, $e/p=0.9$, $L_{\text{jet}} \approx 1.6 \times 10^{45}$ erg/s, $\eta = 1$. c) $B' \approx 20$ G, $D = 15$, $R' \approx 5 \times 10^{15}$ cm, $u'_{\text{phot}} = 3 \times 10^{10}$ eV cm $^{-3}$, $u'_P = 1.9$ erg/cm 3 , $\gamma'_{P,\text{max}} = 4 \times 10^{10}$, $e/p=0.7$, $L_{\text{jet}} \approx 4 \times 10^{45}$ erg/s, $\eta = 1$.

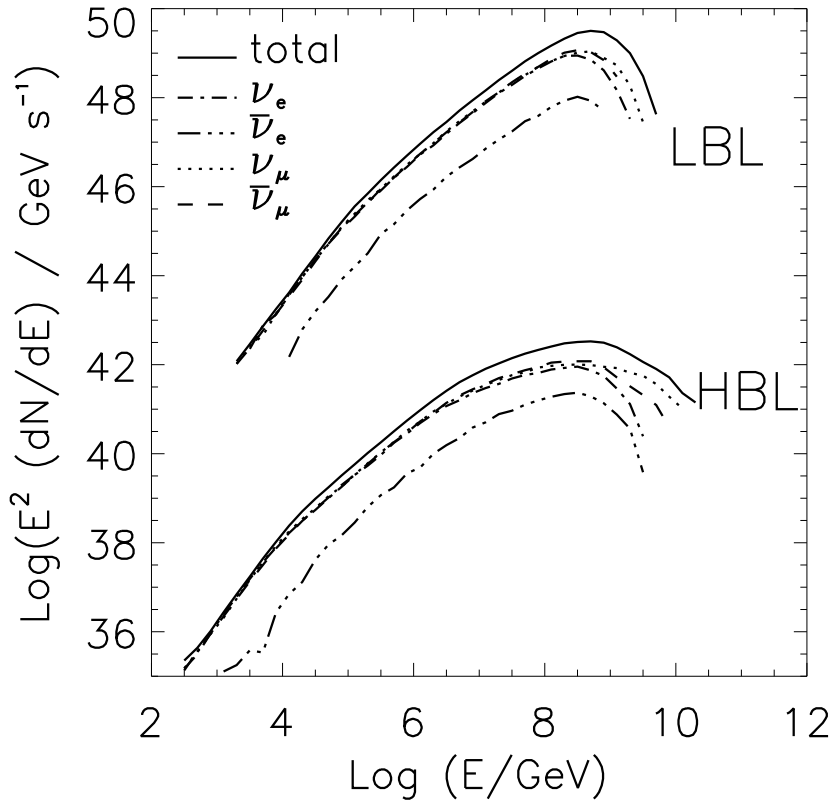


Figure 9: Predicted neutrino output for Mkn 421 (labeled “HBL”) and PKS 0716+714 (labeled “LBL”) as modeled in Fig 6. Antineutrinos from neutron decay are not considered.

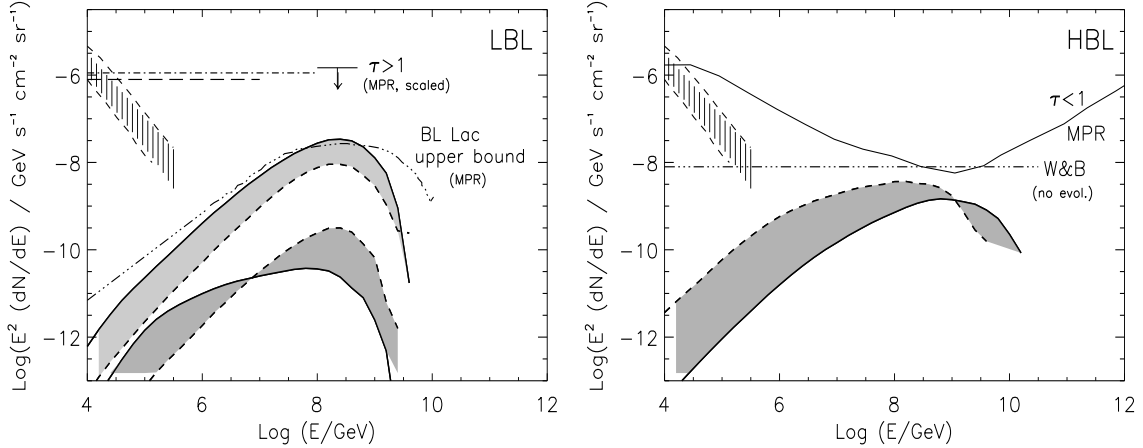


Figure 10: (a) Predicted diffuse $\nu_\mu + \bar{\nu}_\mu$ neutrino spectrum due to LBLs using the predicted BL Lac luminosity function of [40]. The PKS 0716+714/PKS 0537-441 neutrino spectra are used as a template for a typical LBL, and results in a neutrino flux estimate corresponding to the upper/lower shaded area, respectively. The jet frame target photon density u'_{phot} (solid lines) and the “blob” radius R' (dashed lines) are varied to account for the luminosity range in the luminosity function. Antineutrinos from neutron decay are not considered. The hatched area on the left represents the atmospheric neutrino background. Also shown are blazar contributions calculated by Stecker et al. [46] (chain line) and Nellen et al. [47] (dashed constant line). The dashed-dotted line corresponds to the upper bound for BL Lac Objects derived by [36], and takes into account both cosmic rays (neutrons) and gamma-ray emission for these objects. As can be seen it is in excellent agreement with the predictions in the present work. The upper limit arrow above the predicted peak power corresponds to the bolometric bound for sources which are fully opaque ($\tau > 1$) to the emission of cosmic rays as derived in [36], taking into account the bolometric factor of the predicted spectrum. This bound is derived by considering the observed extragalactic γ -ray background only. (b) Predicted diffuse $\nu_\mu + \bar{\nu}_\mu$ neutrino spectrum due to HBLs assuming that 10% of the predicted BL Lac luminosity function of [40] is due to HBLs. The Mkn 421 neutrino spectrum is used as a template for a typical HBL. The jet frame target photon density u'_{phot} (solid lines) and the “blob” radius R' (dashed lines) are varied to account for the luminosity range in the luminosity function. For comparison the upper bound (thin solid line) for sources that are optically thin to cosmic rays ($\tau < 1$) as derived by [36] is shown as well as the upper limit for sources with no evolution as published in [35].